Icarus 328 (2019) 232–245

Contents lists available at ScienceDirect

Icarus

journal homepage: www.elsevier.com/locate/icarus

Global analysis and forecasts of carbon monoxide on Mars

James A. Holmes[a,*], Stephen R. Lewis[a], Manish R. Patel[a,b], Michael D. Smith[c,*]

[a] School of Physical Sciences, The Open University, Milton Keynes MK7 6AA, UK
[b] Space Science and Technology Department, Science and Technology Facilities Council, Rutherford Appleton Laboratory, Harwell Campus, Didcot, Oxfordshire OX11 0QX, UK
[c] NASA Goddard Space Flight Center, Greenbelt, MD 20771, United States

ARTICLE INFO

Keywords:
Mars
Atmosphere
Mars
Data assimilation
Atmospheres
Chemistry

ABSTRACT

Spatial and temporal variations in the Martian carbon monoxide (CO) cycle have been investigated through combining Compact Reconnaissance Imaging Spectrometer for Mars (CRISM) retrievals of carbon monoxide mixing ratio and Mars Climate Sounder (MCS) temperature profiles with a Martian global circulation model (GCM) to produce the first global reanalysis of the Martian CO cycle.

The reanalysis reduces the root mean square error between the forecast and CRISM CO retrievals by a factor of 2–4, dependent on the time of year. Forecasts initiated from the reanalysis show an improved match to standalone CRISM CO retrievals from northern winter solstice to northern summer solstice, indicating the benefit of data assimilation in simulating the CO abundance. The northern summer solstice CO minimum between 10°S – 50°S in the CRISM CO retrievals is found to be caused by a suppression of CO-enriched air leaking from the Hellas and Argyre basins, and is also strongly influenced by the amount of carbon dioxide condensing at the time. The GCM is the first reported to simulate the local CO minimum however it is weaker in strength, as CO-enriched air is also released northward in the area of Argyre basin in the GCM because of a shifted boundary between the southern polar vortex and mid-latitudes. The reanalysis, as a result of the assimilation of MCS temperature profiles, indicates that the polar vortex boundary is northward of Argyre basin and hence no northerly transport of CO-enriched air should be present over this location.

Differences in local CO abundance between the reanalysis and GCM are also evident in spatio-temporal regions where no nearby CRISM CO retrievals are available as a result of alterations in local circulation and the sublimation/condensation of carbon dioxide through the combined assimilation of CRISM CO retrievals alongside MCS temperature profiles, illustrating how constraints can be imposed indirectly on the CO cycle through the powerful technique of data assimilation.

1. Introduction

Carbon monoxide plays an important role in the chemical stability of the Martian atmosphere (McElroy and Donahue, 1972) and has now been observed by a number of ground-based telescopes (Clancy et al., 1990; Krasnopolsky, 2007; Lellouch et al., 1991) and spacecraft in orbit around Mars (Billebaud et al., 2009; Encrenaz et al., 2006; Smith et al., 2009). The long chemical lifetime of CO of around 6 years (Krasnopolsky, 2007) means that for any given annual cycle CO can effectively be treated as a passive tracer. The CO distribution will largely be determined by the dynamical state of the atmosphere and therefore CO can potentially be used as a tracer of the middle atmosphere dynamics.

CO is also a non-condensable species, and hence a relative enhancement in abundance during polar winter is to be expected, as has previously been seen for argon (Sprague et al., 2007). The relative enhancement of CO and other non-condensable gases is directly linked with the condensation of carbon dioxide, and so constraining the CO abundance can be used to study and constrain the sublimation/condensation processes of carbon dioxide. Overestimation of the modelled CO distribution during summer at polar latitudes when compared to retrievals of CO could perhaps be as a result of excessive condensation of carbon dioxide during the preceding winter for example. Based on the above comments, providing a good understanding of the spatio-temporal distribution of CO is therefore a powerful tool for constraining multiple elements of the photochemical and dynamical processes that occur in the Martian atmosphere and investigating annual and inter-annual variations in CO and the middle atmosphere dynamics.

* Corresponding author at: School of Physical Sciences, The Open University, Walton Hall, Milton Keynes MK7 6AA, UK.
E-mail address: james.holmes@open.ac.uk (J.A. Holmes).

https://doi.org/10.1016/j.icarus.2019.03.016
Received 12 October 2018; Received in revised form 22 February 2019; Accepted 13 March 2019
Available online 16 March 2019
0019-1035/

The retrievals of CO column-integrated mixing ratio from the CRISM instrument (Smith et al., 2009) on the Mars Reconnaissance Orbiter (MRO) spacecraft, which by far provide the best spatio-temporal resolution of any available dataset, have recently been extended and updated through improvements in the radiative transfer modelling and algorithm by Smith et al. (2018). New retrievals of CO, including frequent vertical profiles, are also currently being undertaken by instruments on the ExoMars Trace Gas Orbiter (TGO) spacecraft (Korablev et al., 2018; Vandaele et al., 2018). Smith et al. (2018) also provides a detailed comparison of the CRISM retrievals with a simulated CO cycle by the GEM-Mars (Neary and Daerden, 2018) global circulation model. While the general comparison was good, deviations in the observed and simulated cycle were noted such as the inability of the model to replicate a local minimum in CO between 10 − 50°S around northern summer solstice ($L_S = 90°$), a time shift in the annual maximum CO value for different latitudinal regions and excessive increase in CO in the simulation at polar latitudes during early spring (Smith et al., 2018). CO was also treated as a passive tracer in the simulation, and initialised with a globally uniform column-integrated volume mixing ratio of 800 ppm while the observed CO cycle shows significant seasonal variations in the CO abundance.

Providing a consistent temporal and spatial agreement between models and observations of CO is helpful in furthering the understanding of important photochemical and dynamical processes in the Martian atmosphere. To make optimal use of the available information, however, it would be ideal to have the ability to combine the models and retrievals of CO in a self-consistent way. This process would allow for investigation of the evolution of the retrievals that is difficult to deduce for retrievals alone as they include a 'snapshot' of the atmosphere at the exact spatio-temporal location and are generally separated by at least one sol in time. The latter approach provides a much more in-depth investigation of the underlying chemical and physical processes and is one of the primary goals of data assimilation, a technique that combine models and retrievals to provide the best estimate of the global atmospheric state. Other benefits of data assimilation over direct comparison between GCM simulated and observed quantities include providing estimates for parameters which are not directly observed, investigating interactions between chemical species such as CO and water vapour and the ability to combine observational datasets (including of different observations such as CO column mixing ratio and temperature profiles) to optimise the value of the resulting data set.

The good spatio-temporal coverage of CRISM retrievals (Smith et al., 2018) and the retrievals to come from instruments on the ExoMars TGO spacecraft have created the ideal platform for the development of a data assimilation technique for CO retrievals. While the majority of data assimilation studies for Mars have combined retrievals of temperature and/or dust with GCMs (Greybush et al., 2012; Hoffman et al., 2012; Lewis and Barker, 2005; Lewis et al., 2007; Montabone et al., 2006; Navarro et al., 2014a), more recently one particular data assimilation scheme, namely the Analysis Correction (AC) scheme, has also assimilated trace gases such as water vapour/ice (Steele et al., 2014a; Steele et al., 2014b) and ozone (Holmes et al., 2018). CO has never before been assimilated for Mars before, but the assimilation technique is widely used on Earth to investigate the terrestrial CO cycle (Flemming et al., 2017; Gaubert et al., 2017; Inness et al., 2015) primarily to accurately monitor air quality as CO is a pollutant for humans.

In this paper we investigate the effect of CO assimilation using CRISM data and also the inclusion of temperature profiles from the MCS instrument, both on the MRO spacecraft, using a chemically active Mars GCM. Section 2 details the GCM used in this investigation and Section 3 outlines the CRISM CO retrievals and MCS temperature profiles. Details on the assimilation method for both CO retrievals and MCS temperature profiles are documented in Section 4. Section 5 provides the results of the CO and temperature assimilation, and Section 6 states the conclusions of this investigation.

2. Global circulation model

The model simulations conducted as part of this investigation use the UK version of the Laboratoire de Météorologie Dynamique (LMD) Mars GCM (hereafter MGCM). The MGCM is comprised of shared physical parameterisations (Forget et al., 1999) and the LMD photochemical module (Lefèvre et al., 2004) with a recent version of the LMD Mars GCM coupled to a UK-only spectral dynamical core and semi-Lagrangian advection scheme (Newman et al., 2002) and has been developed in a collaboration between the Laboratoire de Météorologie Dynamique, the Open University, the University of Oxford and the Instituto de Astrofisica de Andalucia. The MGCM includes the latest submodels to provide the most realistic modelling of the turbulent processes in the planetary boundary layer (Colaïtis et al., 2013), a water ice cloud microphysics package (Navarro et al., 2014b) that includes radiatively active water ice clouds and supersaturation, and a parameterisation for the enrichment of non-condensable gases (Forget et al., 2008).

Condensation and sublimation of carbon dioxide on the ground and in the atmosphere is calculated from the local temperature and pressure state (Forget et al., 1998). The non-condensable enrichment scheme is fully detailed in Forget et al. (2008), and takes into account the enrichment of lighter gases through a modified convection scheme to simulate the effect of condensation/sublimation of carbon dioxide on non-condensable species through alterations in the molecular mass of the atmosphere. Representation of the northern polar cap includes additional outlying water ice deposits between 120 – 210°E and 75 – 80°N which have previously been shown to provide an improved water vapour peak during northern summer (Steele et al., 2014b).

The coupled LMD photochemical module (Lefèvre et al., 2004) includes up-to-date reaction rates between 16 advected species including carbon dioxide, water vapour and carbon monoxide. Time-varying dust amounts are also taken into account in the photolytic reactions. In terms of chemical reactions, CO is recycled into carbon dioxide by reactions with OH and also re-combination with O. CO does however have a long chemical lifetime as previously mentioned, with the first reaction an order of magnitude slower than the photodissociation of carbon dioxide (10^{-13} s^{-1} as opposed to 10^{-12} s^{-1} for carbon dioxide photodissociation), and the second of these reactions occurring at a rate that is several orders of magnitude slower (less than 10^{-32} s^{-1}) than the first (Lefèvre et al., 2004).

The dust distribution has been prescribed horizontally based on an interpolation of numerous sets of observations from orbiters and landers using a kriging method (Montabone et al., 2015), with a 'semi-interactive' two-moment scheme used to freely transport dust vertically in the model (Madeleine et al., 2011). The model was run at T31 spectral resolution in the horizontal, with a resolution of 5° latitude by 5° longitude for physical and chemical processes and 35 vertical levels in the range 0–110 km. Vertical levels are much closer to one another near the surface and further spread higher in the atmosphere.

3. Data description

This section briefly details the retrievals that are used in the assimilation process, with a complete description of the CRISM hyperspectral CO retrievals and MCS temperature profiles found in Kleinböhl et al. (2017) and Smith et al. (2018) respectively. As a result of the relative sparseness of CRISM retrievals in any given Mars year (MY) and long chemical lifetime of CO, CRISM retrievals from multiple Mars years are combined into a single MY data product. The simulations are conducted for MY 29 as it provides the greatest amount and spatio-temporal coverage of CRISM CO retrievals and MCS temperature profiles for any of the MY covered by the CRISM instrument (see Fig. 1 of Smith et al., 2018 for reference). All of the simulations used for this investigation use the evolving dust distribution (Montabone et al., 2015) for MY 29.

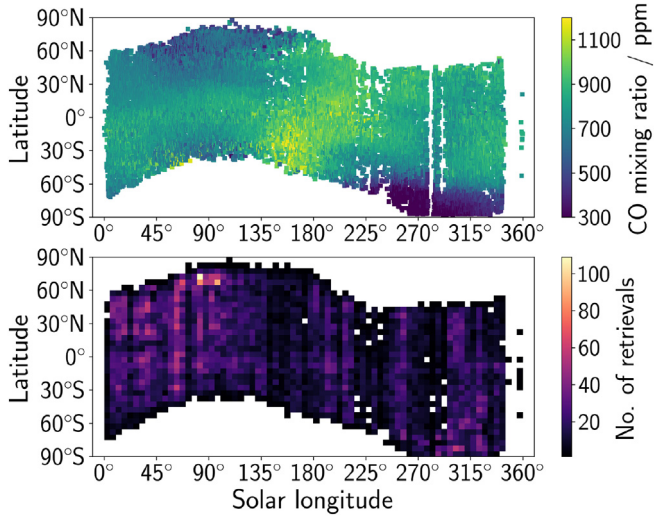

Fig. 1. CRISM column integrated CO mixing ratio retrievals covering multiple Mars years as a function of latitude and solar longitude displaying (a) the column integrated CO mixing ratio and (b) number of retrievals. The number of CRISM CO retrievals are binned every 5°L_S and 5° latitude. White indicates no retrievals.

3.1. CRISM CO retrievals

The CO retrievals assimilated in this study (displayed in Fig. 1a) are from the CRISM instrument on the MRO spacecraft and presented in Smith et al. (2018), with a slightly different set of smoothing parameters used. Due to the Sun-synchronous orbit of the MRO spacecraft, the local time of the CRISM CO retrievals varies from 2 to 4 p.m. for any given retrieval. Also, since the CRISM CO retrievals rely on reflected solar light for signal it is impossible to perform retrievals during the winter season of both hemispheres in the polar region. Maximum column integrated CO mixing ratio values up to around 1300 ppm are seen in mid-latitudes around northern autumnal equinox ($L_S = 180°$) as a result of transported CO-enriched air from the southern polar winter region. Minimum values of column integrated CO mixing ratio reaching as low as 120 ppm are found in southern polar latitudes during northern winter solstice (centred on $L_S = 270°$) as a result of sublimation of carbon dioxide from the southern polar cap during perihelion when the Sun is at its minimum distance from Mars. The more intense solar radiation during southern summer, when compared to northern summer, can account for the more extreme local minimum in column integrated CO mixing ratio observed during southern summer when comparing the polar summer of each hemisphere. A localised minimum of column integrated CO mixing ratio is also apparent between 10 – 50°S around northern summer solstice ($L_S = 90°$), shown more clearly in the binned retrievals in Fig. 3 of (Smith et al., 2018).

The radiative transfer algorithm used to retrieve the column integrated CO mixing ratio along with underlying assumptions and uncertainties is described fully in Smith et al. (2018), and briefly detailed in this section. The outcome of the retrieval process is 26,998 high signal-to-noise ratio CO retrievals covering multiple Mars years. The ground resolution at pericentre is around 2 km^2, with an average calculated uncertainty in column integrated CO mixing ratio of 40% after accounting for systematic errors in the assumptions and approximations used in the retrieval process (Smith et al., 2018). The CRISM CO retrievals used in this study are retrieved using an improved retrieval algorithm compared to the CRISM retrievals detailed in Smith et al. (2009) and have undergone a robust quality control procedure, with nadir-viewing hyperspectral observations only included with an emission angle and solar incidence angle of 80° or less (Smith et al., 2018).

3.2. MCS 2-D retrievals of atmospheric temperature

The MCS instrument, also on the MRO spacecraft, employs a nearly continuous limb viewing strategy in order to achieve greatly increased sensitivity to minor and trace constituents (McCleese et al., 2007). The MCS instrument is a passive radiometer which retrieves in 9 spectral bands covering the visible and mid-to far-infrared channels. The vertical coverage of the temperature profiles is from the surface up to altitudes of around 85 km and daily spatial coverage is comprised of two sets of twelve narrow strips of data, separated by about 30° in longitude. The actual local time of an observation varies with both latitude and season, which is fully accounted for in the assimilation process, with equator crossings of the instrument close to 3 a.m. and 3 p.m. for the two daily strips of data.

Originally fully described in Kleinböhl et al. (2009), the retrieval of vertical temperature profiles from the MCS measured radiance has recently been updated to consider horizontal gradients in profile retrievals from limb observations of the Martian atmosphere (Kleinböhl et al., 2017). The use of two-dimensional radiative transfer has primarily resulted in a reduction of biases in winter polar regions from 15 to 30 K using spherical symmetry to 2–4 K using this new method. For any general retrieval, the typical error throughout most of the atmosphere is around 0.5 K and increases at higher altitudes due to the reduction in signal-to-noise ratio (> 1 K above 40 km) and in the lower atmosphere in situations where the atmosphere becomes opaque. Fig. 2 displays the number of MCS temperature profiles that are assimilated into the MGCM during the simulations of MY 29, with a total of just over 1.5 million retrievals used. The MCS instrument was switched off after $L_S = 330°$*irc* of MY 29 and hence why the analysis in this study is only conducted until this time, with limited CRISM CO retrievals available after this time period for any of the MY covered by the CRISM CO retrievals included in this study.

4. Overview of the assimilation method

The assimilation of CRISM CO retrievals and MCS temperature profiles is performed in this study using a form of the Analysis Correction (AC) scheme (Lorenc et al., 1991), and has been shown in the past to be a computationally inexpensive and robust method (Lewis et al., 2007). Using this methodology, observations of long-lived species such as CO are combined with the MGCM through successive corrections at every dynamical timestep, resulting in an evolving CO distribution that is supplemented by knowledge of the transport and atmospheric chemistry from a GCM. While other assimilation schemes are also available for use, including a Local Ensemble Transform Kalman Filter (Navarro et al., 2014a), no other assimilation scheme has yet been used to assimilate chemical species. As previously mentioned, the AC scheme is the only current scheme capable of assimilating chemical species on Mars and has successfully assimilated water vapour/ice

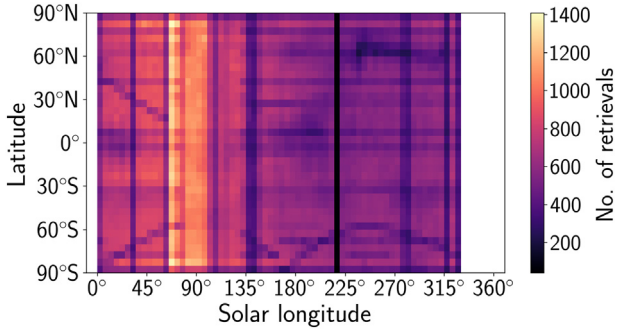

Fig. 2. Number of MCS temperature profiles during MY 29 as a function of latitude and solar longitude. The number of MCS temperature profiles are binned every 5°L_S and 5° latitude. White indicates no retrievals.

(Steele et al., 2014a; Steele et al., 2014b) and ozone (Holmes et al., 2018). While the assimilation of CO retrievals is a first for Mars in this study, attempts to combined GCMs with CO observations have previously been performed for Earth (Clerbaux et al., 2001; Herron-Thorpe et al., 2012; Inness et al., 2015), primarily to investigate air quality and pollution associated with CO emissions.

The method used to assimilate the MCS temperature retrievals is identical to the method explained in Lewis et al. (2007). The method used to assimilate CRISM CO retrievals is largely similar to the method used by Holmes et al. (2018) and Steele et al. (2014b). CO is considered an active chemical species and so the assimilation method is linked to the LMD photochemical module (Lefèvre et al., 2004), as was the case for the previous assimilation of ozone (Holmes et al., 2018), whilst the previous assimilation studies involving water vapour and ice were conducted by considering them as passive species in a chemical sense. Since the CRISM CO retrievals are column-integrated CO mixing ratio, this quantity is compared like for like with the modelled column-integrated CO mixing ratio during the assimilation process. As there is no information on the vertical profile of CO through the retrievals, and the column-integrated CO mixing ratio needs to be translated into mixing ratio at each vertical level for fully 4-dimensional transport of the chemical species, the CO mixing ratio at each vertical level is scaled using an independent height factor C_i where i is a given model grid point. The CO mass mixing ratio $q_{im}{}^{\text{assim}}$ after assimilation at each model grid point i and layer m is thus updated by

$$q_{im}^{\text{assim}} = C_i q_{im}^{\text{model}}, \quad where \quad C_i = \frac{D_i + \Delta D_i}{D_i} \tag{1}$$

only at grid points i affected by retrievals on the current physics timestep. In the above equation, ΔD_i is the increment applied to the MGCM, taking into account the local time and spatial position of relevant CRISM CO retrievals within the given radius of influence, and D_i is the column-integrated CO mixing ratio simulated by the MGCM.

This method effectively means we assume the vertical profile of CO in the MGCM to be accurate, and is the current best option as a result of minimal retrievals of the CO vertical profile available at this time. The unconstrained vertical profile of CO is a potential source for CO differences identified using this scaling method, but since CO is largely passive and the dynamics are constrained in the reanalysis by the MCS temperature profiles, we expect sources of error in the vertical profile to be minimal. The validity of an independent height factor will be explored in the future through comparison with retrievals of the vertical profile of CO with retrievals from instruments on the ExoMars TGO spacecraft tepvandaele18,korablev18, with the assimilation of CO vertical profiles also planned for the future to remove this potential source of error.

Experiments to decide on the best insertion parameters for the data were conducted for the CRISM CO retrievals through calculation of the average root mean square error (RMSE) of column integrated CO mixing ratio for several times of year and across a range of different time windows and choosing the combination of parameters which returned the lowest RMSE when the different simulations were compared to one another and the control. For dust opacity and temperature assimilation, a 6 h time window (5 h ahead of the observation, and 1 h after) were used since the fields are relatively slow to vary in time (Lewis et al., 2007), with maximal weighting of any given retrieval at its precise local time. The same time window was also decided when assimilating water vapour (Steele et al., 2014b) and shortened by 1 h for the assimilation of ozone, which can have large variations over short timescales (Holmes et al., 2018). The long chemical lifetime of CO resulted in a 7-hour time window (6 h before and 1 h after) found to be optimal, although the RMSE values varied little for a 6-hour or 7-hour time window (average global RMSE value is 42.36 ppb and 42.24 ppb respectively).

The second adjustable insertion parameter is the radius of influence of each retrieval. This parameter was kept at the same value of 3.5S, where S is a correlation scale in km that varies over the time window, shown in Fig. 1 of Lewis et al. (2007), and is equivalent to the CRISM CO retrievals influencing around 1200 km (or around 8 model grid points at the equator centred on the retrieval) at the valid time of the observation. Increasing the radius of influence could result in the incorrect spread of data into regions containing strong gradients of CO, a point noted by Steele et al. (2014b). The assimilation scheme also gives the ability to weight in increasing favour to either the MGCM simulated column integrated CO mixing ratio or CRISM CO retrievals if one of the two sources of information is known to contain larger errors. For this first assimilation of Martian CO, and as a result of the calculated error of around 40% for the CRISM retrievals, the error ratio has been set to unity meaning that the MGCM forecast variations, based on all previous observations forecast forward by the model, are considered comparable in magnitude to uncertainties in the latest observational data.

5. Results

For this investigation, three different simulations are run using the MGCM. The ‘control’ simulation does not include any retrievals, the ‘reanalysis’ includes the assimilation of both CRISM CO retrievals and MCS temperature profiles to produce our best global estimate of the CO cycle on Mars using the AC data assimilation scheme, and the ‘T-reanalysis’ assimilates MCS temperature profiles only. All simulations are started at $L_S = 0^\circ$ in MY 29 and finish at $L_S = 332^\circ$ in MY 29 to allow for a direct comparison between each different simulation (no MCS temperature retrievals are present after $L_S = 330^\circ$ and minimal CRISM CO retrievals are also found after this time, hence why a full annual cycle is not conducted for this study). The initial conditions for each simulation are identical, and come from a reanalysis of CRISM CO retrievals and MCS temperature profiles ran for the entire of MY 29.

5.1. Global CO reanalysis

The number of CRISM CO retrievals assimilated each sol is shown in Fig. 3a, indicating a reasonably large variability of CRISM CO retrievals across the time period of the simulations ($L_S = 0$–332° MY 29). The globally averaged root mean square (RMS) error in column integrated CO mixing ratio for both the reanalysis and control simulation from the CRISM CO retrievals are shown in Fig. 3b, with the reanalysis successful in reducing the RMS error by around a factor of 2 in the first half of the year, and up to 4 in the second half of the year. The only gap in CRISM CO retrievals is seen from $L_S = 280$–285°, with the reanalysis able to forecast a much better fit to the retrievals once they return when compared to the control simulation, although the RMS error is increased in both cases from the most recent value before the observational gap. This is in contrast to the assimilation of total ozone (Holmes et al., 2018), in which the RMS error reverted to the control simulation rapidly as a result of the active nature of ozone in the Martian atmosphere.

The zonally-averaged column integrated CO mixing ratio at 3 p.m. local time in the reanalysis for $L_S = 0$–332° MY 29 is displayed in Fig. 4. Values are given at 3 p.m. local time everywhere to provide an optimal average comparison to CRISM CO retrievals (Fig. 1a). The general annual CO cycle found in the retrievals is well replicated in the reanalysis, with the annual minimum in CO found at southern polar latitudes during southern summer and a mid-latitude CO annual maximum appearing just before northern autumnal equinox ($L_S = 180^\circ$). Maximum global annual values of the column integrated CO mixing ratio are found at southern polar latitudes during southern winter, with values peaking at around 2150 ppm. A local minimum in CO is also simulated between $10 - 50^\circ$S just after northern summer solstice ($L_S = 90^\circ$), to match the minimum found in the CRISM CO retrievals.

The summer depletion of CO is simulated to be stronger in southern summer when compared to northern summer, as also indicated by the CRISM CO retrievals (Fig. 1) and replicated in previous GCM results

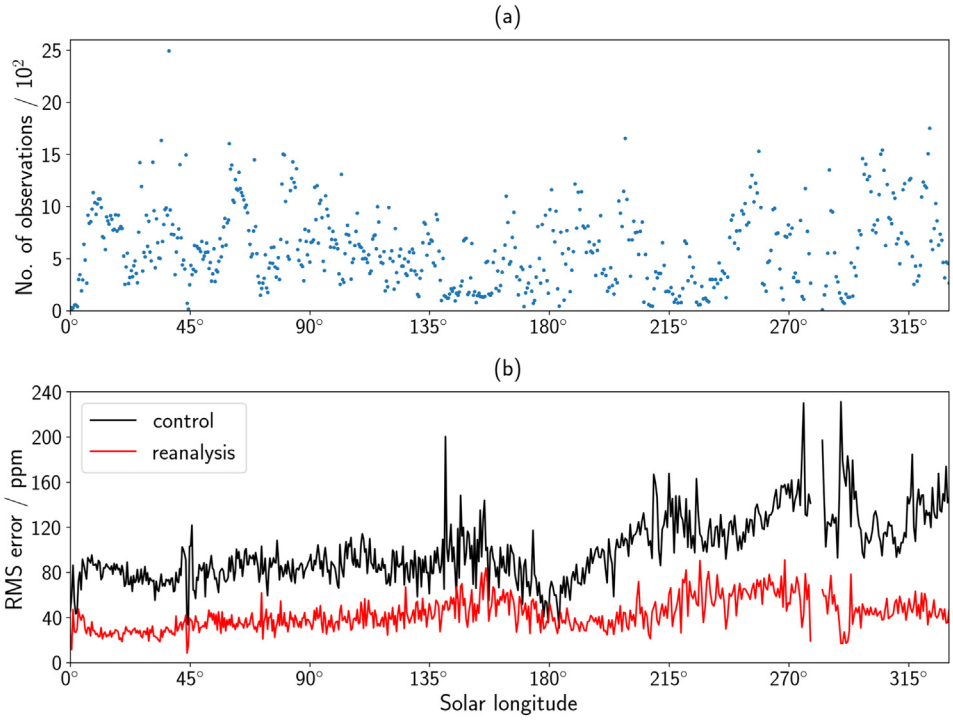

Fig. 3. (a) The number of daily CRISM CO retrievals assimilated in the reanalysis and (b) the daily RMS error in column integrated CO mixing ratio in the control (black) and reanalysis (red) simulation covering $L_S = 0–332^\circ$ MY 29. (For interpretation of the references to colour in this figure legend, the reader is referred to the web version of this article.)

(Smith et al., 2018). Fig. 5a and b show the zonally-averaged column integrated CO mixing ratio at 3 p.m. local time in the control simulation for $L_S = 0–332^\circ$ MY 29 and the deviation from the reanalysis respectively. For the majority of the spatio-temporal region in which CRISM CO retrievals are locally assimilated, deviations of the control simulation from the reanalysis are < 15% and even < 5% particularly in the first half of MY 29 in Fig. 5b. This deviation is far below the retrieval error calculated for the CRISM CO retrievals (Smith et al., 2018), suggesting that the retrieval errors are too conservative. The minimum in CO between 10 – 50°S just after northern summer solstice ($L_S = 90^\circ$) in Fig. 5a is less clear when compared to the reanalysis, but a local CO minimum is clearly present and was not found in the previous comparison with a Mars GCM (Smith et al., 2018). The only location in which the deviations of the control simulation from the reanalysis exceed 40% are in regions in which there are no nearby CRISM CO retrievals and at southern polar latitudes around peak southern summer ($L_S = 270^\circ$), where the relative abundance of CO is affected by the amount of carbon dioxide and water vapour sublimating from the southern polar ice cap. Both of these deviations will be explored in the following sections.

The long chemical lifetime of CO in the Martian atmosphere means that once retrievals are assimilated, any deviations from the control simulation are evolved forwards in time by the MGCM, highlighting the benefit of using a data assimilation method. This is particularly noticeable in regions where CRISM CO retrievals are not found nearby i.e. in the polar winter regions. For southern polar winter, while more CO is found locally at the start of southern polar winter, less relative CO is found locally in the peak of southern polar winter (Fig. 5b) as a result of changes in carbon dioxide condensation through the assimilation of MCS temperature profiles. The latitudinal gradient of CO abundance is also different between the reanalysis and control around $L_S = 225^\circ$ below 60°S This is in contrast to the northern polar winter, where the reanalysis simulates higher CO relative abundance and this is subsequently maintained throughout northern polar winter.

To provide a comparison of the reanalysis and the control simulation with the CRISM CO retrievals focusing initially on several latitude bands, the evolving column-integrated CO mixing ratio for all three sources of information are shown in Fig. 6 using a similar method to

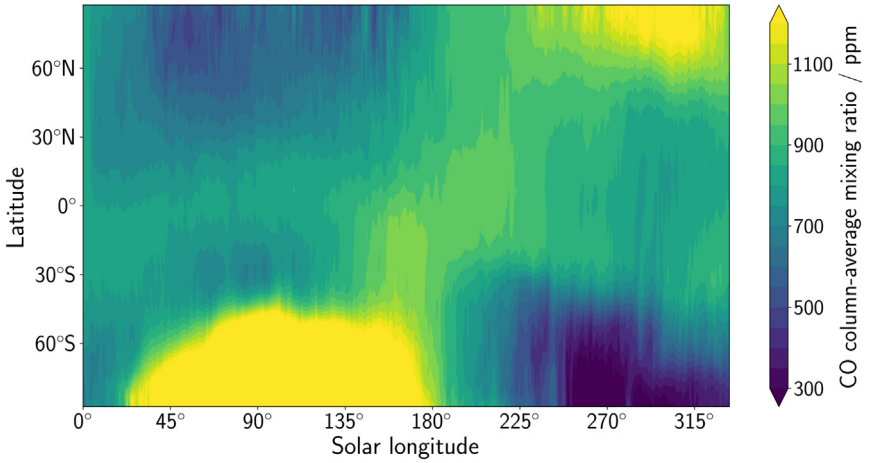

Fig. 4. Zonally-averaged column integrated CO mixing ratio at 3 p.m. everywhere in the reanalysis for $L_S = 0–332^\circ$ MY 29.

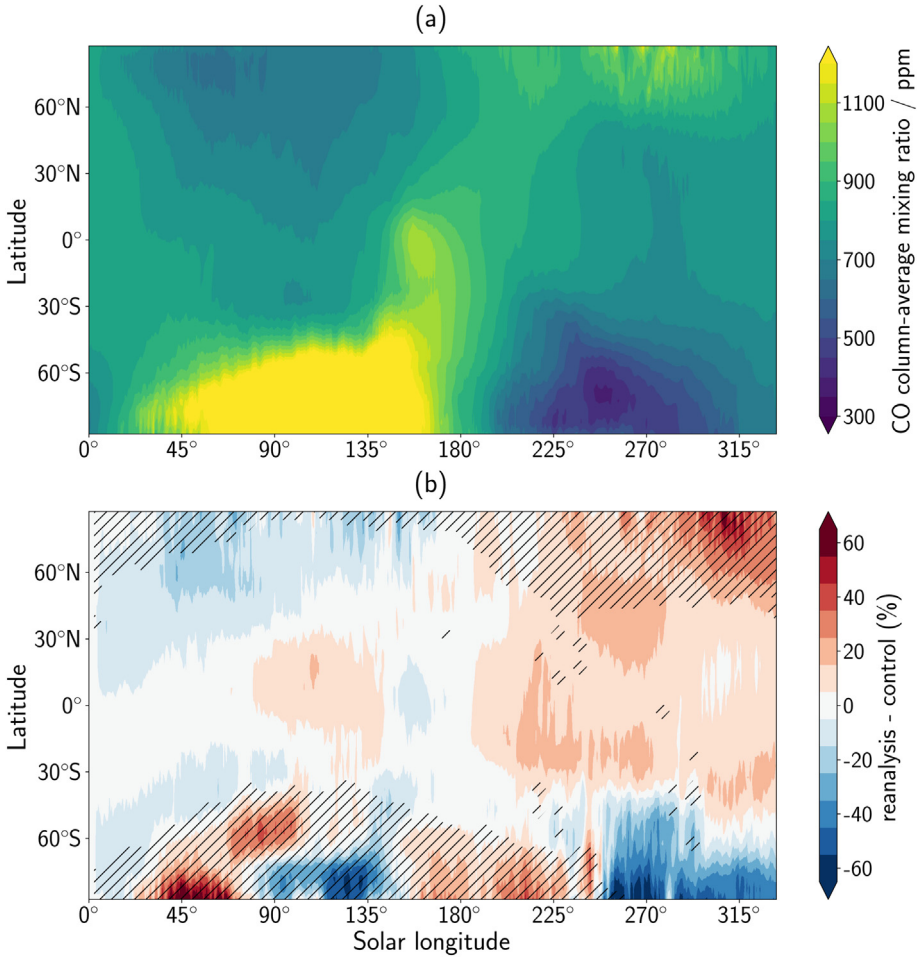

Fig. 5. Zonally-averaged column integrated CO mixing ratio at 3 p.m. everywhere in the control simulation (a) and the percentage difference (reanalysis - control) between the reanalysis and control simulation (b) for $L_S = 0–332^\circ$ MY 29. Percentage is split in 10% intervals with white indicating ± 5%. Hatching indicates regions where there are no nearby CRISM CO retrievals in the spatio-temporal area.

Fig. 11 in Smith et al. (2018). The model dataset includes data for 3 p.m. local time only, and is averaged over all longitudes, 20° of latitude and 5° of L_S. The retrievals are averaged over the same latitude and L_S bands, but may potentially only cover a sample of longitudes based on the orbit track at the time. The reanalysis (blue line in Fig. 6) is effective at providing an optimal CO cycle that is constrained by the CRISM CO retrievals, and is also able to evolve the CRISM CO retrievals to predict the CO abundance in regions where no CRISM CO retrievals are available (see $L_S = 185–360^\circ$ from 70 – 90°N for instance). Information from the assimilation of CRISM CO retrievals in the past is clearly carried forward in time, a powerful advantage of the assimilation technique, as can be seen for example with the difference in CO abundance of around 150 ppm between the reanalysis and control simulation maintained from $L_S = 220–332^\circ$ in the 50 – 70°N latitude band. The primary region in which the control simulation is unable to converge with the CRISM CO retrievals, although the reanalysis is successful in doing so, is in Fig. 6 at southern polar latitudes (70 – 90°S) from $L_S = 240–332^\circ$, although the gradient of the increase in CO abundance does display a good match with the CRISM CO retrievals in time.

One region in which the reanalysis struggles to converge with the CRISM CO retrievals is from $L_S = 225–310^\circ$ in the 30 – 50°S latitude band, although for the majority of time it is still within the retrieval error of 100 ppm (Smith et al., 2018). This is related to the assimilation of MCS temperature profiles, as a reanalysis using only CRISM CO retrievals (not shown) provides a much reduced deviation between the reanalysis and CRISM CO retrievals. The T reanalysis is similar to the control during this time period and location, suggesting that the discrepancy is likely to be caused by errors in either the sublimation of carbon dioxide, the vertical profile of CO, or excessive spreading of lower CRISM CO retrievals northward. Vertical profiles of CO, such as to be returned imminently from the NOMAD instrument on the ExoMars TGO spacecraft, will be a vital piece of knowledge to investigate the identified discrepancy further.

In the Mars GCM comparison conducted by Smith et al. (2018) the main points were that the GCM was unable to correctly simulate the annual maximum of CO at the correct time primarily for northern latitudes, with a maximum time shift of almost 60° L_S from 50 – 70°N, and that the Mars GCM was too quick to build up CO after summer depletion in the northern hemisphere. Fig. 6 indicates that our MGCM does not display any time shift at all in the maximum CO abundance for 50 – 70°N when compared to the CRISM CO retrievals, and this is generally the case for all latitude bands. The increase in relative CO abundance from $L_S = 45–180^\circ$ in the 70 – 90°N latitude band also follows a similar gradient and CO level to the increase found in the CRISM CO retrievals.

To investigate the effect of the MCS temperature profiles assimilated into the MGCM on the surface pressure cycle (and therefore on condensation/sublimation of carbon dioxide), a comparison between the control, reanalysis and CRISM retrievals is presented in Fig. 7. For the majority of locations and times, the general pattern in the control and reanalysis follow the CRISM retrievals well, with at times the control providing a much reduced bias over the majority of latitudinal bands (see $L_S = 90–220^\circ$ in the 10 – 30°N latitude band for example). The surface pressure cycle is tuned when no assimilation is included, and

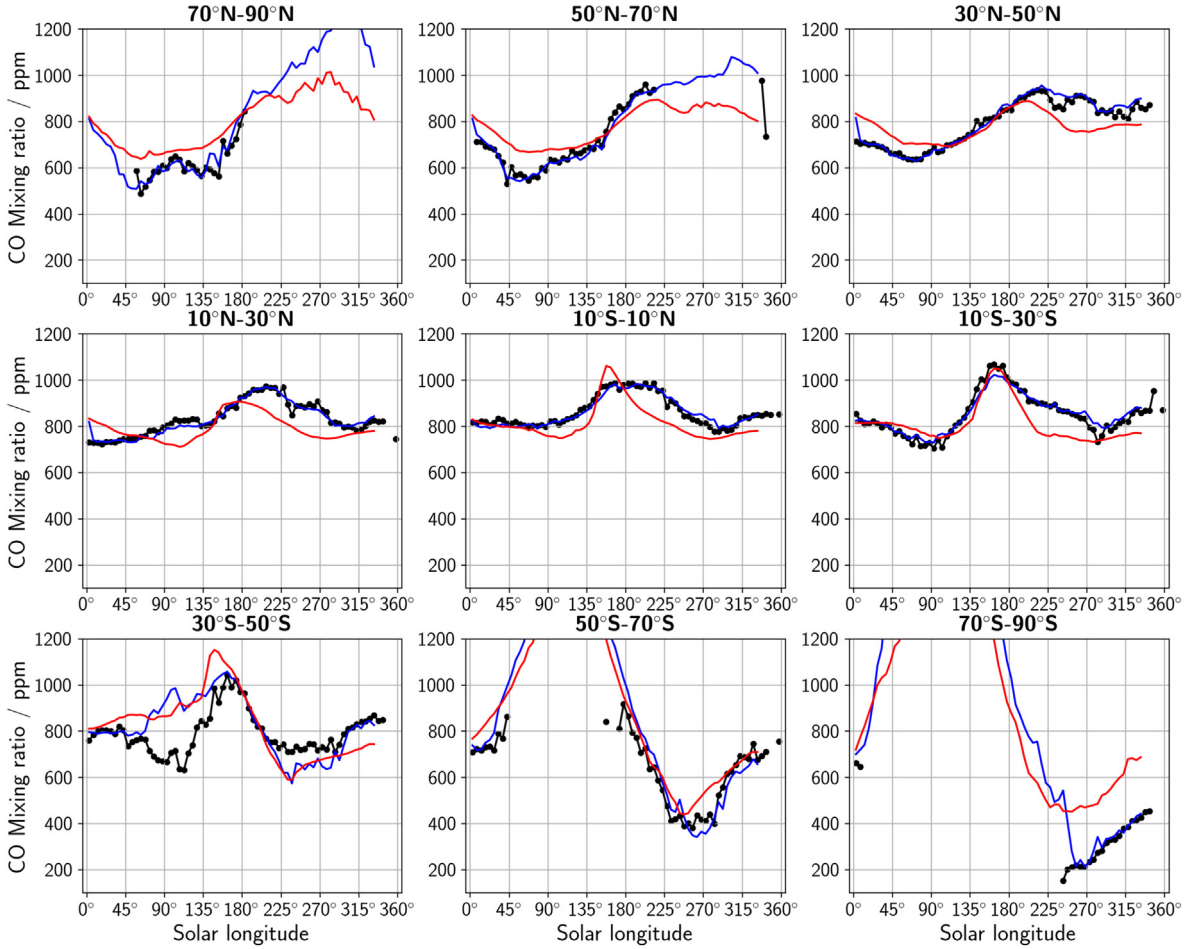

Fig. 6. Comparison of the column integrated CO mixing ratio at 3 p.m. everywhere in the control simulation (red) and reanalysis (blue) with CRISM CO retrievals (black dots) for $L_S = 0–332^\circ$ MY 29. The estimated uncertainty in the binned retrievals is 100 ppm (Smith et al., 2018). (For interpretation of the references to colour in this figure legend, the reader is referred to the web version of this article.)

the assimilation of MCS temperature profiles will alter the surface pressure through temperature alterations and the effect on carbon dioxide condensation/sublimation. The largest difference in surface pressure between the control/reanalysis and the CRISM surface pressure retrievals is in the northern polar region, where the MGCM tends to underestimate the surface pressure.

The spikes in the CRISM surface pressure retrievals are linked to extremes in topography at each latitude band. For example, the spike in the CRISM surface pressure retrievals at $L_S = 145–55^\circ$ in the 30–50°S latitude band are because the majority of CRISM surface pressure retrievals are found in Hellas basin which will display a much higher surface pressure than the majority of other longitudes in this latitudinal band (hence why the control and reanalysis also show a lower surface pressure when averaged over all longitudes).

5.2. Forecasting of the CO column abundance

While the main focus of this study is to explore the differences between the column integrated CO mixing ratio in the reanalysis and control simulation, it is also possible to investigate the skill of the data assimilation system in initialising a forecast for the column integrated CO mixing ratio. For this case study, a forecast of CO is ran for 30 sols at four different time periods throughout the year starting with initial conditions from the reanalysis. The free-running model simulations are then compared to CRISM CO retrievals which have been witheld (along with MCS temperature profiles) from the forecasts over the whole 30 sol time period. By comparing the forecast simulations with results from the control and reanalysis simulation, we can identify if a more realistic initial CO distribution leads to a better model forecast and how quickly the forecast deviates from the reanalysis.

Fig. 8 displays the daily RMS error of the forecast, control and reanalysis from the CRISM CO retrievals for the four different forecast time periods selected. For each forecast simulation, the RMS error is increased after the first sol of simulation, but for the majority of the forecast simulations it is still far below the RMS error from the control (i.e. the free-running simulation). The forecast simulations which start at $L_S = 9^\circ$ MY 29 and $L_S = 282^\circ$ MY 29 (Fig. 8a and d respectively) have a lower RMS error when compared to the control simulation for the whole 30 sol time period, indicating that there is some skill in the global forecasting of column integrated CO mixing ratio during southern summer and early northern spring.

For all four forecast simulations, the RMS error at the end of the 30 sol period is lower than the RMS error for the control simulation, meaning that the initialisation from a reanalysis, that included past CRISM CO retrievals and MCS temperature profiles, is preferable to a free-running model (i.e. the control simulation). The global forecasting skill for $L_S = 92–105^\circ$ and $L_S = 183–201^\circ$ in MY 29 is lower than for the other two forecast simulations, with the forecast RMS error much closer to the control simulation in Fig. 8b and c. During this time period, forecasting of the CO distribution is likely to be heavily linked to the structure of the southern polar vortex, which will play a role initially in maintaining the northern summer solstice CO minimum and also in the leaking of CO from the southern polar region.

The distribution of CO after a 30 sol forecast starting at $L_S = 282^\circ$ MY

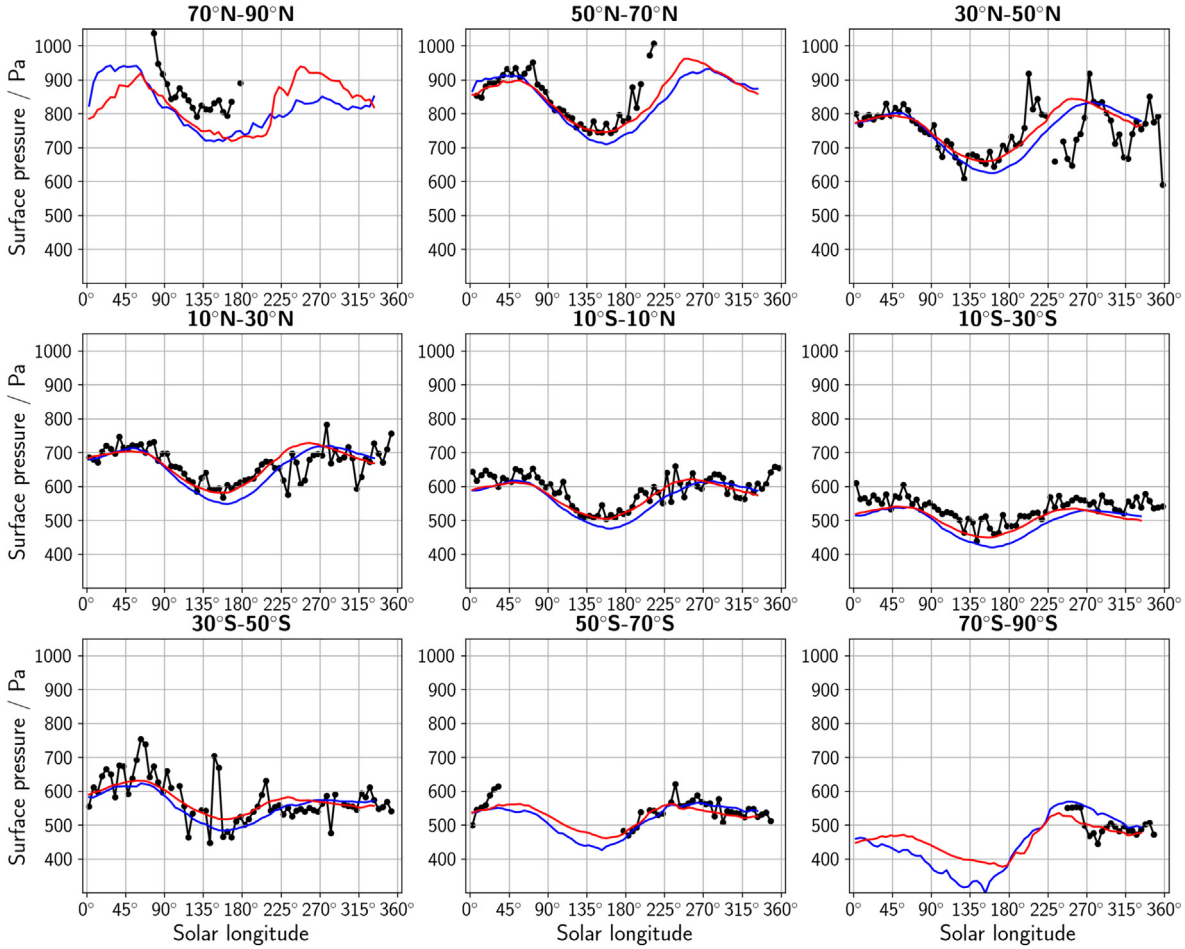

Fig. 7. Comparison of the surface pressure at 3 p.m. everywhere in the control simulation (red) and reanalysis (blue) with CRISM CO retrievals (black dots) for $L_S = 0–332^\circ$ MY 29. (For interpretation of the references to colour in this figure legend, the reader is referred to the web version of this article.)

29 can be seen in Fig. 9b. The magnitude of the southern summer CO depletion is much more inline with the reanalysis (Fig. 9c) than the standalone control (Fig. 9a), with levels dropping to < 300 ppm compared to around 500 ppm in the control simulation.

5.3. The northern summer solstice CO minimum

As previously mentioned, the northern summer solstice mid-latitude CO minimum in the control simulation is reasonably well represented in the MGCM used for this study but not found in a previous comparison of retrievals with a different Mars GCM (Smith et al., 2018). The two possible causes for the CO minimum seen in the reanalysis, and to a less extent in the control simulation, are through chemical reactions or a dynamical process. As previously mentioned in the introduction, the long chemical lifetime of CO suggests that the northern summer solstice CO minimum is the result of the dynamical movements of CO.

The spatial distribution of the column integrated CO mixing ratio averaged over $L_S = 95–100^\circ$ in the reanalysis, control simulation and deviations from the reanalysis are displayed in Fig. 10a, b and c respectively. The local CO minimum centred on a latitude of 30°S is clearly formed by spatial variations as a function of longitude, with CO-enriched air located in Hellas basin (Fig. 10a), but lower CO abundance covering all other longitudes except Hellas basin. The results match the longitudinal variations seen in the CRISM CO retrievals at a similar time of year (see Fig. 5 of Smith et al., 2018). The longitudinal variation in CO abundance at 30°S in the control simulation (Fig. 10b) is marginally different, with lower CO abundance south of the Tharsis Montes and Elysium Mons in good agreement with the reanalysis, however an overestimation of CO is present in particular on the northern edge of Hellas basin and north east of the Argyre basin. There is a general dichotomy in the spatial variations of the deviations of CO column integrated CO mixing ratio from the reanalysis when compared to the control simulation (Fig. 10b), with generally a 20% underestimation in CO abundance in mid-latitudes, and 20% overestimation or higher in CO abundance at polar latitudes. Longitudinal variations exist in the deviations also, with northern polar CO abundance primarily overestimated in the control simulation in the Acidalia Planitia region (20 – 80°W, 50 – 80°N), and good agreement at the majority of other longitudes in the same latitude band.

The cause of the local CO minimum in Fig. 10a is suppression of CO-enriched air leaking from the northern edge of Hellas and Argyre basins, combined with negligible release from all other longitudes. Fig. 11a and b show streamlines of the winds in the lowest 10 km of the atmosphere (where the majority of CO is located at this time of year in the southern hemisphere) for the reanalysis and control simulation respectively averaged over $L_S = 90–105^\circ$. Assimilation of thermal profiles from MCS results in alterations to the dynamical state of the atmosphere (through thermal wind balance) and has been shown to be robust in predicting actual transient wave behaviour (Lewis et al., 2007).

Alterations to the dynamics in the reanalysis through the assimilation of MCS temperature profiles lead to changes in the strength and in some cases the direction of the meridional winds, and also a shift in the southern polar vortex boundary. For the reanalysis in Fig. 11a, meridional transport in the southern hemisphere is strengthened, with increased southward transport located over the north-eastern edge of the Argyre basin as opposed to marginally northward transport seen in the

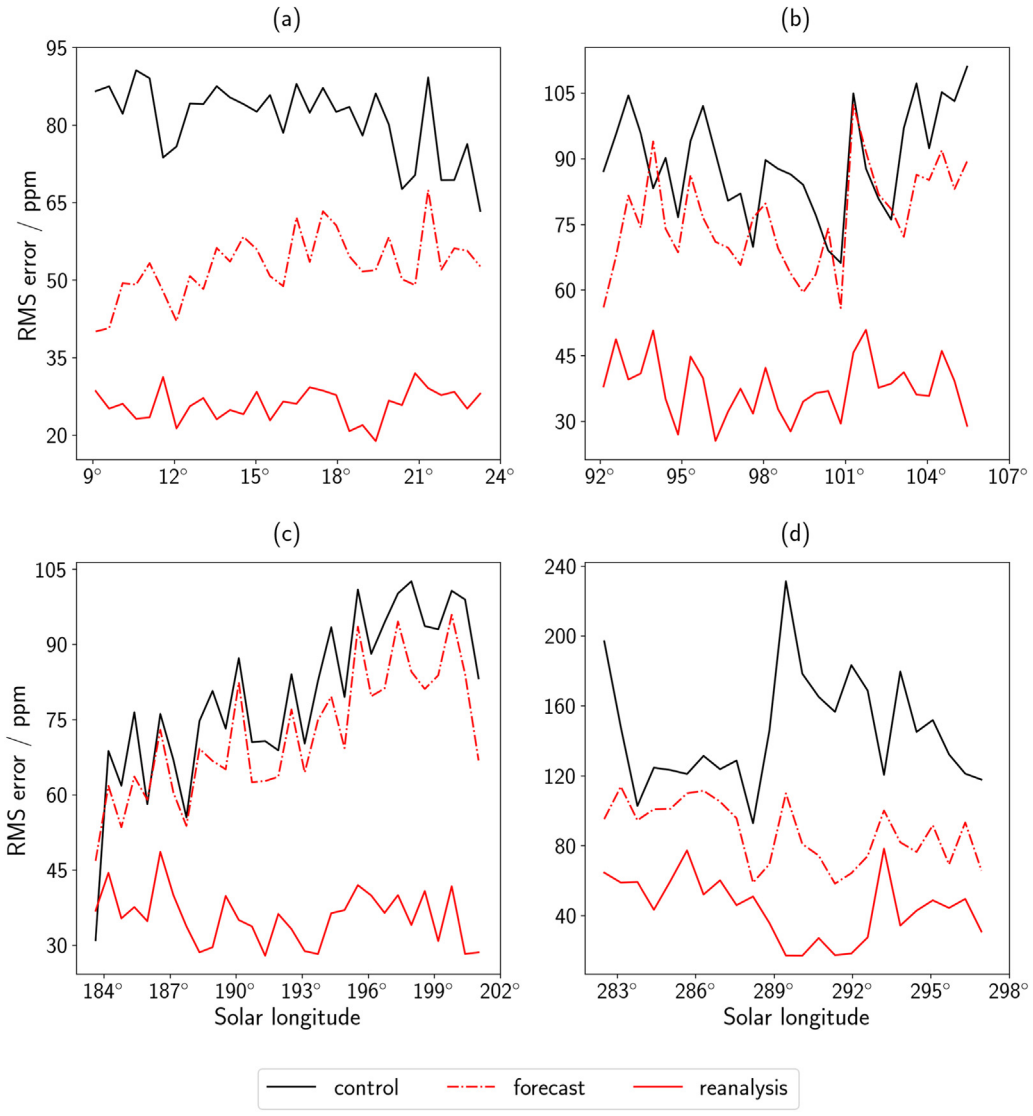

Fig. 8. The daily RMS error in column integrated CO mixing ratio in the control (black), reanalysis (red) and forecast (red dashed) simulation covering (a) $L_S = 9–23^\circ$ MY 29, (b) $L_S = 92–105^\circ$ MY 29, (c) $L_S = 183–201^\circ$ MY 29 and (d) $L_S = 282–297^\circ$ MY 29. Note the different scales for RMS error. (For interpretation of the references to colour in this figure legend, the reader is referred to the web version of this article.)

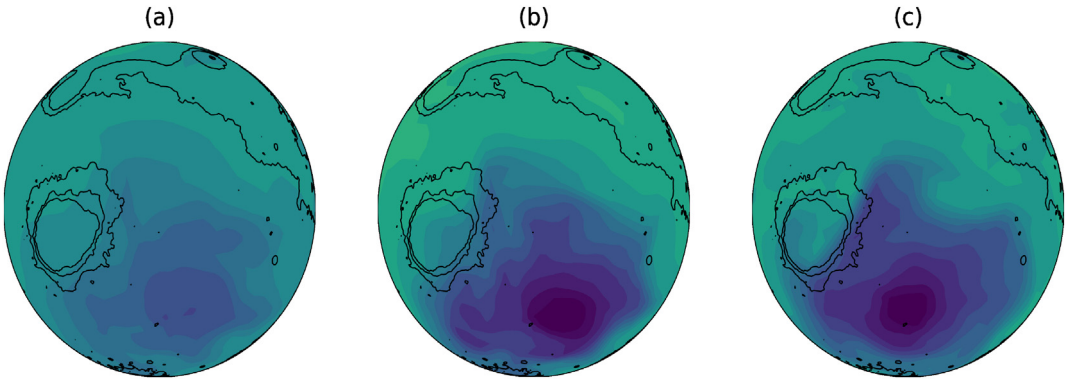

Fig. 9. The simulated column integrated CO mixing ratio in the (a) control, (b) forecast and (c) reanalysis at $L_S = 297^\circ$ MY 29 after 30 sols of withheld CRISM CO retrievals (i.e. simulations started at $L_S = 282^\circ$ MY 29). Black contours indicate topography.

control simulation (Fig. 11b). In the control simulation at this time of year (Fig. 11b), the primary locations for transport of CO-enriched air at southern polar latitudes is seen to be from Hellas basin, however northward meridional winds are also apparent on the western edge of the Argyre basin. At latitudes northward of 20°S, the meridional transport is northward across all longitudes, and therefore the northern summer solstice CO minimum seen in the reanalysis, the control simulation and the CRISM CO retrievals can largely be explained by

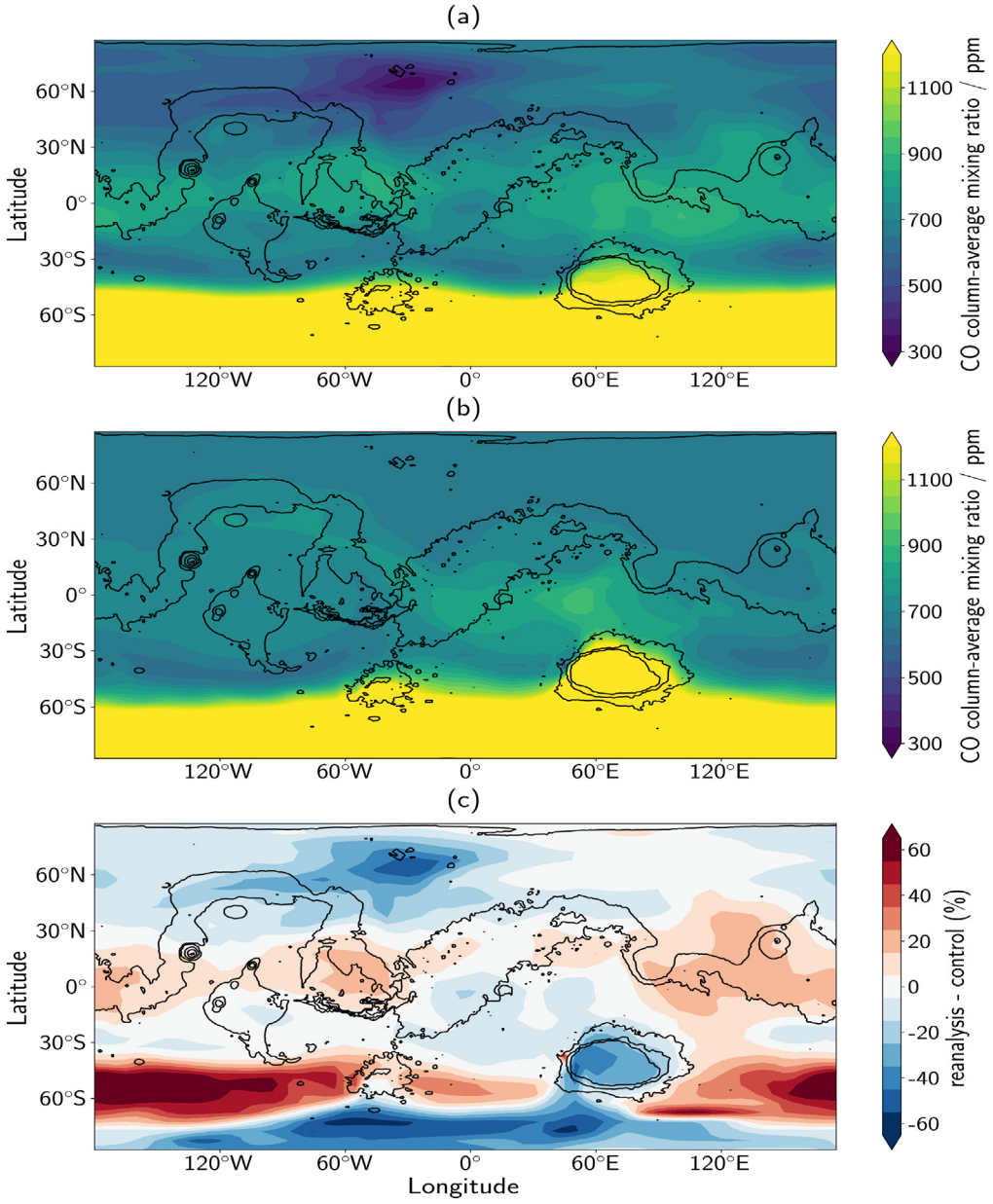

Fig. 10. Longitude-latitude maps of the column integrated CO mixing ratio in the reanalysis (a), control (b) and the percentage difference (reanalysis - control) between the reanalysis and control simulation (c) averaged over $L_S = 95–100^{\circ}$ MY 29.

dynamics. The cut-off of northward transport of CO-enriched air from the western edge of the Argyre basin in the reanalysis as a result of a shift in the southern polar vortex boundary (Fig. 11a), which contributes to raising the local CO abundance north-east of the Argyre basin in the control simulation (Fig. 10b), explains why the northern summer solstice CO minimum is not seen for an extended period of the year in the control simulation as is observed in the reanalysis displayed in Fig. 4 and also in the CRISM CO retrievals.

Dynamics alone cannot fully explain the northern summer solstice CO minimum however, since the reanalysis finds it difficult to converge with the CRISM CO retrievals from $L_S = 75–135^{\circ}$ in the 30 – 50°S latitude band in Fig. 6. The vertical structure of CO during $L_S = 90–105^{\circ}$ MY 29 in the reanalysis, T-reanalysis and control are shown in Fig. 12a, b and c respectively. When assimilating MCS temperature profiles only, the northern summer solstice CO minimum disappears as a result of enhanced condensation of carbon dioxide at higher altitudes over the southern pole (Fig. 12b) when compared to the control (Fig. 12c), that is subsequently transported by the equator-crossing anti-clockwise Hadley circulation. This is suppressed in the reanalysis through lower CO abundance at around 30°S in the middle atmosphere (Fig. 12a) by the additional assimilation of CRISM CO retrievals.

The carbon dioxide condensation/sublimation scheme is tuned for when no temperature retrievals are assimilated, and MCS temperature profiles retrieve a lower temperature above the south pole at this time of year, hence why CO is relatively increased in the reanalysis and T-reanalysis by increased carbon dioxide condensation. Vertical profiles of CO, such as those to be returned by the NOMAD instrument on the ExoMars TGO spacecraft will be vital in determining if the carbon dioxide condensation is indeed too strong when MCS temperature profiles are assimilated. Over-excessive carbon dioxide condensation is also the cause for increased CO abundance in regions where no CRISM CO retrievals are found in the southern polar region of Fig. 5a from $L_S = 30–90^{\circ}$ and Fig. 11b.

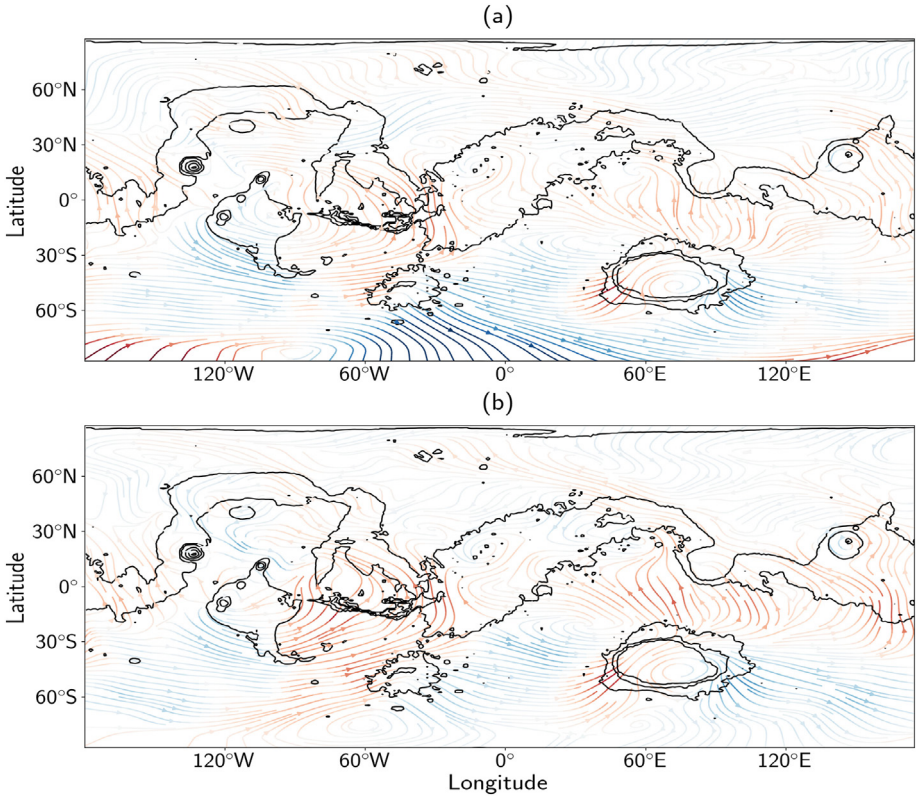

Fig. 11. Longitude-latitude maps of wind streamlines from the (a) reanalysis and (b) control simulation, averaged over $L_S = 90–105^\circ$ MY 29. The divergent colours of the streamline indicate northerly (blue) or southerly (red) meridional winds, with darker colours indicating stronger meridional winds. (For interpretation of the references to colour in this figure legend, the reader is referred to the web version of this article.)

5.4. Southern summer CO depletion and vertical structure

The primary region of disagreement between the reanalysis and the control simulation is during peak southern summer at southern polar latitudes (see Fig. 5b). The MGCM has a tendency to deviate from the local water vapour column retrieved by the Thermal Emission Spectrometer (TES) instrument (see Fig. 4 of Holmes et al., 2018), however sensitivity tests in which the local water vapour column was increased to match TES retrievals had minimal effect on the CO abundance, as expected from the slow chemical reaction rates (Lefèvre et al., 2004).

During perihelion at southern polar latitudes, carbon dioxide is sublimating from the southern polar cap and so an overestimation of CO in the control simulation could be linked to insufficient sublimation of carbon dioxide. Fig. 13a and c display the zonally averaged vertical structure of CO mixing ratio for the reanalysis and control respectively. The CO mixing ratio peaks at high altitudes above the southern pole in both simulations (although higher altitude CO contributes less to the column integrated CO mixing ratio as a result of the smaller differences in pressure), with minimal amounts of CO near the surface as to be expected for both the control simulation and the reanalysis. The near

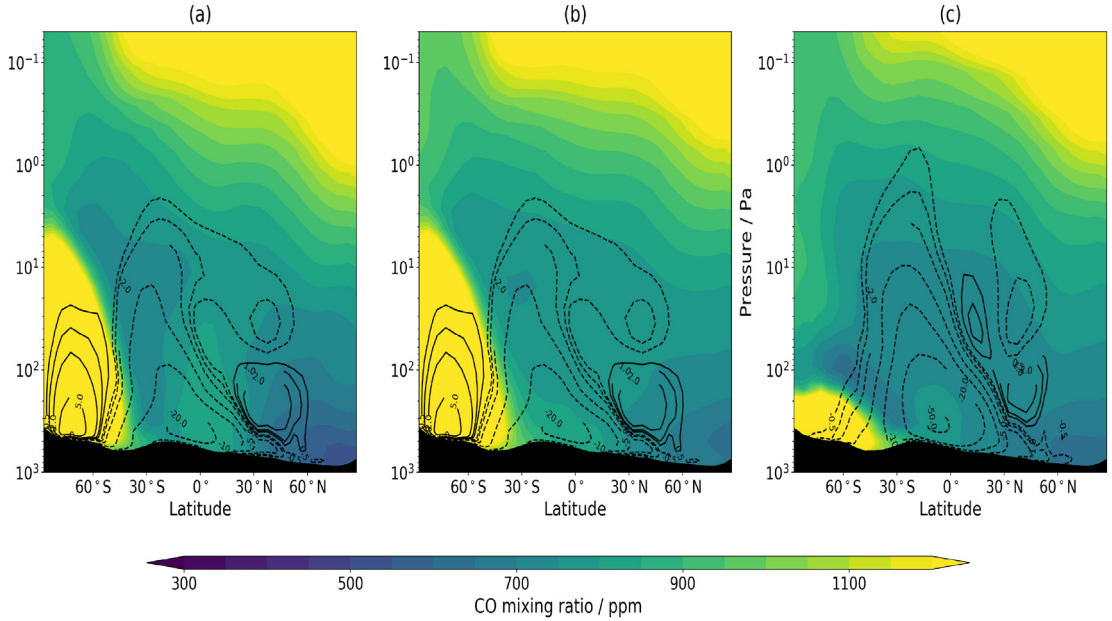

Fig. 12. Zonally-averaged vertical structure of CO mixing ratio at 3 p.m. everywhere in the (a) reanalysis, (b) T-reanalysis and (c) control for $L_S = 90–105^\circ$ MY 29. Black contours indicate the meridional stream function, with solid/dashed indicating clockwise/anti-clockwise motion, with units of 10^8 kg s^{-1}.

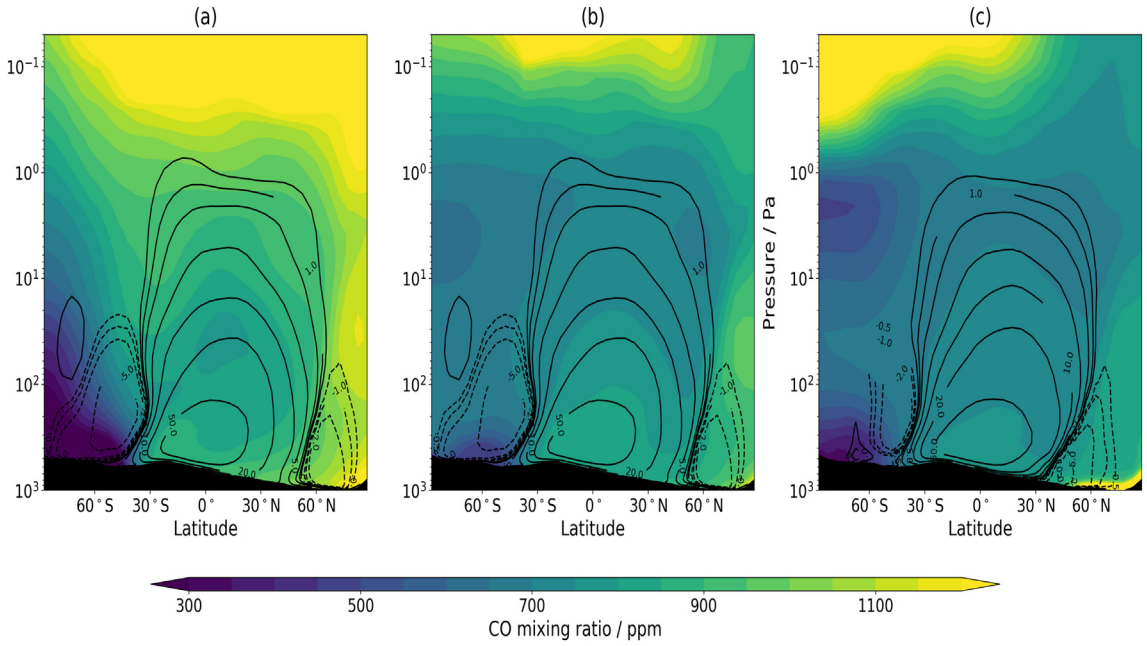

Fig. 13. Zonally-averaged vertical structure of CO mixing ratio at 3 p.m. everywhere in the (a) reanalysis, (b) T-reanalysis and (c) control for $L_S = 260–280^\circ$ MY 29. Black contours indicate the meridional stream function, with solid/dashed indicating clockwise/anti-clockwise motion, with units of 10^8 kg s^{-1}.

surface CO mixing ratio in the reanalysis (Fig. 13a) is decreased when compared to the control simulation in Fig. 13c and also extends to higher southern latitudes.

The retrieval procedure for CRISM CO observations relies on the assumption of a well-mixed vertical profile, and Fig. 13a suggests this to potentially not be the case in the region where we see the largest disagreement between the reanalysis and control simulation. The assumption of a well-mixed vertical profile can therefore potentially explain some of the disagreement in CO column-average mixing ratio during southern polar latitudes at southern summer in Fig. 5b. It is important to remember that when assimilating the CRISM CO retrievals an independent height factor is used, the validity of which is currently undetermined. Ideally, the vertical profile of CO predicted by the MGCM would be compared to retrievals of the CO vertical profile or even also assimilated into the MGCM, a process which is entirely possible with the assimilation scheme. Retrievals of the CO vertical profile will soon become available from NOMAD and ACS on the ExoMars TGO spacecraft (Korablev et al., 2018; Vandaele et al., 2018), providing an ideal dataset to explore alterations to the CO vertical profile seen when assimilating MCS temperature profiles in the reanalysis.

Alterations to the carbon dioxide sublimation at this time of the year as a result of the assimilation of MCS temperature profiles also impacts on the southern summer CO depletion. The T-reanalysis in Fig. 13b simulates increased CO abundance in the southern polar region when compared to the control (Fig. 13c) as a result of potentially an excessive relative abundance of CO at the end of southern polar winter. The surface pressure of the reanalysis at this time in the 70 – 90°S latitude band in Fig. 7 is in reasonable agreement with the CRISM surface pressure, so this points to an excess of CO present leading into this time period being the cause (as can be seen from $L_S = 150–250^\circ$ in Fig. 5b). Indeed, further evidence that points to the initial excess of CO being the cause can be seen in Fig. 9, which indicates that a forecast with initial conditions of reduced CO in southern summer provides a much better match to the reanalysis for the southern summer depletion. As mentioned previously, the condensation and sublimation of carbon dioxide is tuned for when no MCS temperature profiles are assimilated, and so alterations in the atmospheric temperature will alter how much carbon dioxide condenses/sublimates, with lower surface pressure throughout most of southern polar winter in the reanalysis when compared to the control in Fig. 7 (although no CRISM surface pressure retrievals are available to determine whether the reanalysis or control is a more accurate simulation in this spatio-temporal region).

A secondary effect of assimilation of MCS temperature profiles along with CRISM CO retrievals in the reanalysis is that the CO abundance in regions in which there are no nearby CRISM CO retrievals can still be different to a restricted reanalysis that includes only the assimilation of MCS temperature profiles. The differences are as a result of the transport of CO-enriched air as shown in the comparison of northern polar CO abundance in the reanalysis and T-reanalysis in Fig. 13a and b respectively. The T-reanalysis and control underestimate the column integrated CO mixing ratio in mid-latitude regions during the second half of the year (see Fig. 5b for a reanalysis-control comparison). As a result of the independent height factor and the majority of CO being found in the upper atmosphere, the increased mid-latitude CO abundance due to CRISM CO retrievals is transported northwards by the overturning circulation to produce the increased CO over the northern polar region. The differences in the column integrated CO mixing ratio are partially linked to alterations in local amounts of condensing carbon dioxide, as can be identified in the surface pressure difference between the reanalysis and control in the 70 – 90°N latitude band from $L_S = 220–315^\circ$ in Fig. 7. However, transport of CO must also play a role in the distribution shown in the reanalysis, otherwise the distribution in the northern polar region of the reanalysis and T-reanalysis would be identical if it only depended on alterations in the condensation of carbon dioxide.

The inclusion of MCS temperature profiles along with CRISM CO retrievals illustrates how the assimilation of multiple different datasets during the assimilation process can help constrain CO indirectly. For example, by assimilating the MCS temperature profile, it affects the CO abundance in regions that are unobserved by CRISM through either alterations in carbon dioxide condensation/sublimation or transport from observed regions, or both. If another dataset of surface pressure was available in the region unobserved region by CRISM and it compares favourably with the reanalysis, we can be more confident that the CO prediction is better than a standalone model simulation.

6. Conclusions

Retrievals of column integrated CO mixing ratio from the CRISM instrument and MCS temperature profiles have been assimilated into the UK version of the LMD GCM to provide the first global reanalysis of the CO cycle and investigate the processes which lead to spatio-temporal variations in CO.

The reanalysis reduces the globally averaged RMS error in column integrated CO mixing ratio by a factor of 2 to 4, with an increased reduction in the second half of the Mars year. The primary region in which differences in column integrated CO mixing ratio are seen between the reanalysis and MGCM that are outside the CRISM retrieval error is at southern polar latitudes around perihelion, where CO is depleted as carbon dioxide sublimates from the southern polar cap. The reanalysis suggests that the MGCM possibly under-predicts the strength of carbon dioxide sublimation, but coincident vertical profiles of CO are warranted to confirm the result as for these assimilation experiments an independent height factor is used to scale CO vertically using the column CO value from the CRISM retrievals.

The inclusion of MCS temperature profiles along with CRISM CO retrievals in the assimilation process leads to a more accurate representation of the temperature structure and circulation of the atmosphere that can alter the distribution of CO in unobserved regions, alongside alterations to the condensation/sublimation of carbon dioxide. This is a powerful method to provide constraints on predictions of CO in regions that are unobserved due to instrument limitations, and when compared to vertical profiles of CO from instruments such as NOMAD on the ExoMars TGO spacecraft, can help to constrain the carbon dioxide condensation/sublimation cycle. The modelled vertical distribution of CO is also found to be altered through additional assimilation of MCS temperature profiles, and will be the focus of future observations and reanalysis.

The potential to forecast the CO abundance using the data assimilation method has been explored by comparing forecasts initiated from the reanalysis at different times of year with withheld CRISM CO retrievals. The forecast simulations which start at $L_S = 9^\circ$ MY 29 and $L_S = 282^\circ$ MY 29 had a lower RMS error when compared to the control simulation for the whole 30 sol time period, indicating that there is some skill in the global forecasting of column integrated CO mixing ratio during southern summer and early northern spring.

The northern summer solstice CO minimum between $10^\circ - 50^\circ$S is found to be caused by suppression of CO-enriched air leaking from the northern edge of Hellas basin and strongly linked to carbon dioxide condensation during this time period. The northern summer solstice CO minimum is maintained for an extended time period via this mechanism, with the southern polar vortex boundary preventing leaking of CO-enriched air from all other longitudes, including the Argyre basin.

The MGCM is the first reported Mars GCM able to replicate a northern summer solstice CO minimum, albeit a weaker feature as a result of modelling deficiencies in the positioning of the southern polar vortex boundary. The modelling deficiency results in additional release of CO-enriched air from the Argyre basin region dampening the CO minimum. The MGCM also shows a minimal time difference in the annual CO mixing ratio at different latitude bands and a reasonable match to the observed increase in CO at northern polar latitudes in the time period after aphelion, both found to be issues in a previous GCM comparison with the CRISM CO retrievals (Smith et al., 2018).

The assimilation package associated with the UK version of the LMD GCM is now capable of assimilating multiple different trace gases and other meteorological variables such as temperature and dust, an invaluable tool for investigating links between the different components and transport processes in the Martian atmosphere and for combining future observations from the ExoMars TGO spacecraft.

Acknowledgements

JAH, SRL and MRP gratefully acknowledge the support of the STFC/UK Space Agency under grant ST/R001405/1; SRL and MRP also thank UKSA for support under grants ST/P001262/1 and ST/S00145X/1. MDS acknowledges support from the Mars Reconnaissance Orbiter project. We are grateful for an ongoing collaboration with François Forget and coworkers at LMD.

References

Billebaud, F., Brillet, J., Lellouch, E., Fouchet, T., Encrenaz, T., Cottini, V., Ignatiev, N., Formisano, V., Giuranna, M., Maturilli, A., Forget, F., 2009. Observations of CO in the atmosphere of Mars with PFS onboard Mars Express. Planet. Space Sci. 57, 1446–1457.

Clancy, R.T., Muhleman, D.O., Berge, G.L., 1990. Global changes in the 0-70 KM thermal structure of the Mars atmosphere derived from 1975 to 1989 microwave CO spectra. J. Geophys. Res. 95, 14543–14554.

Clerbaux, C., Hadji-Lazaro, J., Hauglustaine, D., MéGie, G., Khattatov, B., Lamarque, J.-F., 2001. Assimilation of carbon monoxide measured from satellite in a three-dimensional chemistry-transport model. J. Geophys. Res. 106, 15.

Colaïtis, A., Spiga, A., Hourdin, F., Rio, C., Forget, F., Millour, E., 2013. A thermal plume model for the Martian convective boundary layer. J. Geophys. Res. Planets 118, 1468–1487.

Encrenaz, T., Fouchet, T., Melchiorri, R., Drossart, P., Gondet, B., Langevin, Y., Bibring, J.-P., Forget, F., Bézard, B., 2006. Seasonal variations of the Martian CO over Hellas as observed by OMEGA/Mars Express. Astron. Astrophys. 459, 265–270.

Flemming, J., Benedetti, A., Inness, A., Engelen, R.J., Jones, L., Huijnen, V., Remy, S., Parrington, M., Suttie, M., Bozzo, A., Peuch, V.-H., Akritidis, D., Katragkou, E., 2017. The CAMS interim reanalysis of carbon monoxide, ozone and aerosol for 2003-2015. Atmos. Chem. Phys. 17, 1945–1983.

Forget, F., Hourdin, F., Talagrand, O., 1998. CO_2 snowfall on Mars: simulation with a general circulation model. Icarus 131, 302–316.

Forget, F., Hourdin, F., Fournier, R., Hourdin, C., Talagrand, O., Collins, M., Lewis, S.R., Read, P.L., Huot, J.-P., 1999. Improved general circulation models of the Martian atmosphere from the surface to above 80 km. J. Geophys. Res. 104, 24155–24176.

Forget, F., Millour, E., Montabone, L., Lefèvre, F., 2008. Non condensable gas enrichment and depletion in the Martian polar regions. In: Third International Workshop on the Mars Atmosphere: Modeling and Observations, pp. 9106 Vol. 1447 of LPI Contributions.

Gaubert, B., Worden, H.M., Arellano, A.F.J., Emmons, L.K., Tilmes, S., Barré, J., Martinez Alonso, S., Vitt, F., Anderson, J.L., Alkemade, F., Houweling, S., Edwards, D.P., 2017. Chemical feedback from decreasing carbon monoxide emissions. Geophys. Res. Lett. 44, 9985–9995.

Greybush, S.J., Wilson, R.J., Hoffman, R.N., Hoffman, M.J., Miyoshi, T., Ide, K., McConnochie, T., Kalnay, E., 2012. Ensemble Kalman filter data assimilation of thermal emission spectrometer temperature retrievals into a Mars GCM. J. Geophys. Res. 117, 11008.

Herron-Thorpe, F.L., Mount, G.H., Emmons, L.K., Lamb, B.K., Chung, S.H., Vaughan, J.K., 2012. Regional air-quality forecasting for the Pacific northwest using MOPITT/TERRA assimilated carbon monoxide MOZART-4 forecasts as a near real-time boundary condition. Atmos. Chem. Phys. 12, 5603–5615.

Hoffman, M.J., Eluszkiewicz, J., Weisenstein, D., Uymin, G., Moncet, J.-L., 2012. Assessment of Mars atmospheric temperature retrievals from the thermal emission spectrometer radiances. Icarus 220, 1031–1039.

Holmes, J.A., Lewis, S.R., Patel, M.R., Lefèvre, F., 2018. A reanalysis of ozone on Mars from assimilation of SPICAM observations. Icarus 302, 308–318.

Inness, A., Blechschmidt, A.-M., Bouarar, I., Chabrillat, S., Crepulja, M., Engelen, R.J., Eskes, H., Flemming, J., Gaudel, A., Hendrick, F., Huijnen, V., Jones, L., Kapsomenakis, J., Katragkou, E., Keppens, A., Langerock, B., de Maziere, M., Melas, D., Parrington, M., Peuch, V.H., Razinger, M., Richter, A., Schultz, M.G., Suttie, M., Thouret, V., Vrekoussis, M., Wagner, A., Zerefos, C., 2015. Data assimilation of satellite-retrieved ozone, carbon monoxide and nitrogen dioxide with ECMWF's composition-IFS. Atmos. Chem. Phys. 15, 5275–5303.

Kleinböhl, A., Schofield, J.T., Kass, D.M., Abdou, W.A., Backus, C.R., Sen, B., Shirley, J.H., Lawson, W.G., Richardson, M.I., Taylor, F.W., Teanby, N.A., McCleese, D.J., 2009. Mars climate sounder limb profile retrieval of atmospheric temperature, pressure, and dust and water ice opacity. J. Geophys. Res. Planets 114, 10006.

Kleinböhl, A., Friedson, A.J., Schofield, J.T., 2017. Two-dimensional radiative transfer for the retrieval of limb emission measurements in the Martian atmosphere. J. Quant. Spectrosc. Radiat. Transf. 187, 511–522.

Korablev, O., Montmessin, F., Trokhimovskiy, A., Fedorova, A.A., Shakun, A.V., Grigoriev, A.V., Moshkin, B.E., Ignatiev, N.I., Forget, F., Lefèvre, F., Anufreychik, K., Dzuban, I., Ivanov, Y.S., Kalinnikov, Y.K., Kozlova, T.O., Kungurov, A., Makarov, V., Martynovich, F., Maslov, I., Merzlyakov, D., Moiseev, P.P., Nikolskiy, Y., Patrakeev, A., Patsaev, D., Santos-Skripko, A., Sazonov, O., Semena, N., Semenov, A., Shashkin, V., Sidorov, A., Stepanov, A.V., Stupin, I., Timonin, D., Titov, A.Y., Viktorov, A., Zharkov, A., Altieri, F., Arnold, G., Belyaev, D.A., Bertaux, J.L., Betsis, D.S., Duxbury, N., Encrenaz, T., Fouchet, T., Gérard, J.-C., Grassi, D., Guerlet, S., Hartogh, P., Kasaba, Y., Khatuntsev, I., Krasnopolsky, V.A., Kuzmin, R.O., Lellouch, E., Lopez-Valverde, M.A., Luginin, M., Määttänen, A., Marcq, E., Martin Torres, J., Medvedev, A.S., Millour, E., Olsen, K.S., Patel, M.R., Quantin-Nataf, C., Rodin, A.V.,

Shematovich, V.I., Thomas, I., Thomas, N., Vazquez, L., Vincendon, M., Wilquet, V., Wilson, C.F., Zasova, L.V., Zelenyi, L.M., Zorzano, M.P., 2018. The atmospheric chemistry suite (ACS) of three spectrometers for the ExoMars 2016 trace gas orbiter. Space Sci. Rev. 214, 7.

Krasnopolsky, V.A., 2007. Long-term spectroscopic observations of Mars using IRTF/CSHELL: mapping of O_2 dayglow, CO, and search for CH_4. Icarus 190, 93–102.

Lefèvre, F., Lebonnois, S., Montmessin, F., Forget, F., 2004. Three-dimensional modeling of ozone on Mars. J. Geophys. Res. 109, 7004.

Lellouch, E., Paubert, G., Encrenaz, T., 1991. Mapping of CO millimeter-wave lines in Mars' atmosphere - the spatial variability of carbon monoxide on Mars. Planet. Space Sci. 39, 219–224.

Lewis, S.R., Barker, P.R., 2005. Atmospheric tides in a Mars general circulation model with data assimilation. Adv. Space Res. 36, 2162–2168.

Lewis, S.R., Read, P.L., Conrath, B.J., Pearl, J.C., Smith, M.D., 2007. Assimilation of thermal emission spectrometer atmospheric data during the Mars Global Surveyor aerobraking period. Icarus 192, 327–347.

Lorenc, A.C., Bell, R.S., MacPherson, B., 1991. The Meteorological Office analysis correction data assimilation scheme. Q. J. R. Meteorol. Soc. 117, 59–89.

Madeleine, J.-B., Forget, F., Millour, E., Montabone, L., Wolff, M.J., 2011. Revisiting the radiative impact of dust on Mars using the LMD Global Climate Model. J. Geophys. Res. Planets 116, E11010.

McCleese, D.J., Schofield, J.T., Taylor, F.W., Calcutt, S.B., Foote, M.C., Kass, D.M., Leovy, C.B., Paige, D.A., Read, P.L., Zurek, R.W., 2007. Mars climate sounder: an investigation of thermal and water vapor structure, dust and condensate distributions in the atmosphere, and energy balance of the polar regions. J. Geophys. Res. Planets 112, 5.

McElroy, M.B., Donahue, T.M., 1972. Stability of the Martian atmosphere. Science 177, 986–988.

Montabone, L., Lewis, S.R., Read, P.L., Hinson, D.P., 2006. Validation of Martian meteorological data assimilation for MGS/TES using radio occultation measurements. Icarus 185, 113–132.

Montabone, L., Forget, F., Millour, E., Wilson, R.J., Lewis, S.R., Cantor, B., Kass, D., Kleinböhl, A., Lemmon, M.T., Smith, M.D., Wolff, M.J., 2015. Eight-year climatology of dust optical depth on Mars. Icarus 251, 65–95.

Navarro, T., Forget, F., Millour, E., Greybush, S.J., 2014a. Detection of detached dust layers in the Martian atmosphere from their thermal signature using assimilation. Geophys. Res. Lett. 41, 6620–6626.

Navarro, T., Madeleine, J.-B., Forget, F., Spiga, A., Millour, E., Montmessin, F., Määttänen, A., 2014b. Global climate modeling of the Martian water cycle with improved microphysics and radiatively active water ice clouds. J. Geophys. Res. Planets 119, 1479–1495.

Neary, L., Daerden, F., 2018. The GEM-Mars general circulation model for Mars: description and evaluation. Icarus 300, 458–476.

Newman, C.E., Lewis, S.R., Read, P.L., Forget, F., 2002. Modeling the Martian dust cycle, 1. Representations of dust transport processes. J. Geophys. Res. 107, 5123.

Smith, M.D., Wolff, M.J., Clancy, R.T., Murchie, S.L., 2009. Compact reconnaissance imaging spectrometer observations of water vapor and carbon monoxide. J. Geophys. Res. Planets 114, E00D03.

Smith, M.D., Daerden, F., Neary, L., Khayat, A., 2018. The climatology of carbon monoxide and water vapor on Mars as observed by CRISM and modeled by the GEM-Mars general circulation model. Icarus 301, 117–131.

Sprague, A.L., Boynton, W.V., Kerry, K.E., Janes, D.M., Kelly, N.J., Crombie, M.K., Melli, S.M., Murphy, J.R., Reedy, R.C., Metzger, A.E., 2007. Mars' atmospheric argon: tracer for understanding Martian atmospheric circulation and dynamics. J. Geophys. Res. Planets 112, E03S02.

Steele, L.J., Lewis, S.R., Patel, M.R., 2014a. The radiative impact of water ice clouds from a reanalysis of Mars Climate Sounder data. Geophys. Res. Lett. 41, 4471–4478.

Steele, L.J., Lewis, S.R., Patel, M.R., Montmessin, F., Forget, F., Smith, M.D., 2014b. The seasonal cycle of water vapour on Mars from assimilation of thermal emission spectrometer data. Icarus 237, 97–115.

Vandaele, A.C., Lopez-Moreno, J.-J., Patel, M.R., Bellucci, G., Daerden, F., Ristic, B., Robert, S., Thomas, I.R., Wilquet, V., Allen, M., Alonso-Rodrigo, G., Altieri, F., Aoki, S., Bolsée, D., Clancy, T., Cloutis, E., Depiesse, C., Drummond, R., Fedorova, A., Formisano, V., Funke, B., González-Galindo, F., Geminale, A., Gérard, J.-C., Giuranna, M., Hetey, L., Ignatiev, N., Kaminski, J., Karatekin, O., Kasaba, Y., Leese, M., Lefèvre, F., Lewis, S.R., López-Puertas, M., López-Valverde, M., Mahieux, A., Mason, J., McConnell, J., Mumma, M., Neary, L., Neefs, E., Renotte, E., Rodriguez-Gomez, J., Sindoni, G., Smith, M., Stiepen, A., Trokhimovsky, A., Vander Auwera, J., Villanueva, G., Viscardy, S., Whiteway, J., Willame, Y., Wolff, M., 2018. NOMAD, an integrated suite of three spectrometers for the ExoMars trace gas mission: technical description, science objectives and expected performance. Space Sci. Rev. 214, 80.